ELSEVIER

Cardiovascular Research 33 (1997) 258–271

Cardiovascular Research

Review

Role of wavefront curvature in propagation of cardiac impulse

Vladimir G. Fast *, André G. Kléber

Department of Physiology, University of Berne, Bühlplatz 5, CH-3012 Berne, Switzerland

Received 17 June 1996; accepted 17 October 1996

Abstract

It is traditionally assumed that impulse propagation in cardiac muscle is determined by the combination of two factors: (1) the active properties of cardiac cell membranes and (2) the passive electrical characteristics of the network formed by cardiac cells. However, advances made recently in the theory of generic excitable media suggest that an additional factor—the geometry of excitation wavefronts—may play an important role. In particular, impulse propagation strongly depends on the wavefront curvature on a small spatial scale. In the heart, excitation wavefronts have pronounced curvatures in several situations including waves initiated by small electrodes, waves emerging from narrow tissue structures, and waves propagating around the sharp edges of anatomical obstacles or around a zone of functional conduction block during spiral wave rotation. In this short review we consider the theoretical background relating impulse propagation to wavefront curvature and we estimate the role of wavefront curvature in electrical stimulation, formation of conduction block, and the dynamic behavior of spiral waves.

Keywords: Myocardium; Wave front; Impulse propagation; Conduction; Reentry; Spiral wave

1. Introduction

The mechanisms of impulse propagation in the heart have been extensively studied for several decades both theoretically and experimentally [1–4]. It has been firmly established that impulse propagation is dependent on two tissue properties: (1) *the passive electrical properties* of cardiac muscle defined by the tissue micro-architecture, the cell shapes, the passive membrane characteristics, and the distribution of gap junctions, and (2) *the excitable membrane properties* defined by the distribution, conductances, and kinetic characteristics of ionic channels, transporters, and pumps. From the biophysical point of view, cardiac tissue belongs to the class of so-called 'reaction–diffusion systems' in which a local reaction, such as an action potential, propagates through a medium due to the release of stored biochemical energy. It shares important aspects of its biophysical behavior with a variety of other excitable systems not only of biological, but also of physical and chemical origin [5]. Investigation of these systems, first by means of mathematical modeling and subsequently in experiments, has shown that in addition to the passive and active properties of the medium, a third factor—the *geometry of the excitation wavefront*—contributes to wave propagation [6,7]. Particularly, the *curvature* of a wavefront may cause slowing of propagation and conduction block. Also, wavefront curvature is important for defining the properties of spiral waves which are responsible for some types of cardiac tachyarrhythmias. The concept of wavefront curvature has recently been applied to studies of impulse conduction in cardiac muscle, provoking new experimental and modeling work. The purpose of this short article is to discuss the new data obtained in these studies together with the theoretical background and to evaluate the role of wavefront curvature in normal and abnormal impulse propagation and in the mechanisms of re-entrant excitation. The role of wavefront curvature in the behavior of spiral waves will be discussed in detail.

* Corresponding author. Tel. +41 31 631-87-11; Fax +41 31 631-46-11; E-mail: fast@pyl.unibe.ch

Time for primary review 21 days.

PII S0008-6363(96)00216-7

2. Effects of wavefront curvature on wave propagation

2.1. Wavefront curvature and conduction velocity

The basic mechanism relating wavefront curvature to velocity of propagation (θ) in an excitable medium is illustrated in Fig. 1. For simplicity, the medium is assumed to be 2-dimensional and isotropic; the effects of wavefront curvature in 3-dimensional and in anisotropic media will be considered later. In the case of a flat wavefront, conduction velocity is equal to the steady-state velocity in a one-dimensional strand. The steady-state velocity (θ_0) is solely determined by the passive and active properties of excitable tissue (e.g., Ref. [1]). When the excitation front is curving outward (convex), the conduction velocity is lower than θ_0. This is because the local excitatory current supplied by the cells at the front of a convex wave distributes over a larger membrane area downstream. An opposite process takes place when the excitation front is curving inwards (concave). In this case, excitatory current converges in front of the propagating wave, producing a more rapid membrane depolarization. As a result, the conduction velocity of a concave wavefront is larger than θ_0. The degree of wavefront bending is characterized by the local curvature (ρ) which is defined as the negative reciprocal of the local radius of curvature (r):

$$\rho = -\frac{1}{r}$$

It follows from this definition that the convex front has a negative ρ, the concave front has a positive ρ, and $\rho = 0$ for a flat front. A quantitative description of the dependence of conduction velocity on curvature in a continuous isotropic 2-dimensional excitable medium can be obtained analytically for small values of ρ. Zykov and Morozova [8] have shown that under such conditions the velocity is given by the following equation:

$$\theta = \theta_0 + D\rho \qquad (1)$$

The coefficient D is determined by the passive properties of the medium. For a continuous isotropic model of the electrical structure of cardiac muscle, D is equal to $1/C_m S_v R_i$ where C_m is the specific membrane capacitance, S_v is the cell surface-to-volume ratio, and R_i is the intracellular resistivity.

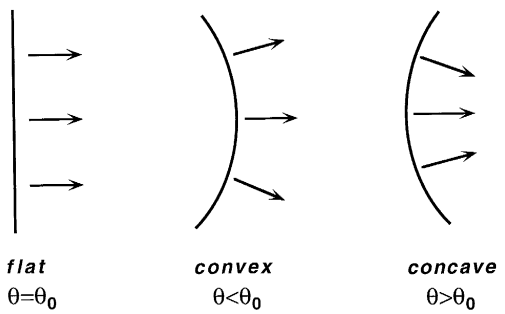

Fig. 1. Effect of wavefront geometry on propagation velocity θ. θ_0 denotes the steady-state velocity in a one-dimensional medium.

2.2. Critical curvature and conduction block

Since conduction velocity decreases as the wavefront curvature becomes more negative, it follows that the velocity will become zero at some critical level of ρ (ρ_c), and the excitation wave will be blocked. Moreover, in the case of a circular nucleus of excitation, propagation will not take place if the radius of the nucleus is less than a critical radius, r_c. A rough theoretical estimate of ρ_c and r_c can be obtained from Eq. (1). Assuming that the linear relationship between the wavefront velocity and the curvature is preserved at high ρ values, the velocity will become zero when ρ and r satisfy the following equations:

$$\rho_c = -\frac{\theta_0}{D} \text{ or } r_c = \frac{D}{\theta_0} \qquad (2)$$

The effects of curvature on wave propagation have been extensively studied in mathematical models [6,7,9–12]. Experimentally, they have been demonstrated in several excitable systems including the chemical Belousov-Zhabotinsky reaction [13,14] and a biological system producing calcium waves in *Xenopus laevis* oocytes [15].

The fact that these effects have been considered only rarely in heart tissue until recently is explained by the small radii at which wavefront curvature significantly affects conduction. In order to estimate quantitatively the effect of ρ on the conduction velocity in ventricular myocardium, we assume R_i to be 400 Ωcm (longitudinal direction [16]), C_m to be 1 $\mu F/cm^2$, and S_v to be 0.33 μm^{-1} [17]. Under such conditions the coefficient D is approximately 0.76 cm^2/s. The propagation velocity (θ_0) of the flat excitation front is approximately 50 cm/s in the longitudinal direction [16,18]. Introducing D and θ_0 into Eq. (2) yields a critical curvature $\rho_c = 66$ cm^{-1} which corresponds to a critical radius of curvature $r_c = 152$ μm. Detection of a circular nucleus of excitation of such a small radius requires a spatial resolution of < 100 μm, which is difficult to achieve by using conventional mapping techniques with arrays of extracellular electrodes. It should be noted that estimates of ρ_c and r_c based on Eq. (2) may include two types of errors: (1) the dependence of θ on ρ in cardiac muscle may be non-linear at high values of ρ and (2) the dependence of θ on ρ may show a discontinuity near ρ_c and, correspondingly, conduction velocity may decrease to zero abruptly. The precise shape of the function $\theta = f(\rho)$ in cardiac tissue is not yet known. Examples of the dependence of θ on ρ for several excitable models (Fig. 2) suggest that the true value for the critical curvature may be somewhat smaller and the critical radius larger than predicted by Eq. (2).

An important factor affecting wave propagation in ventricular myocardium is its 3-dimensional (3D) structure. The theory linking conduction velocity to wavefront curvature according to Eq. (1) is valid for the 3D case as well. However, the relation between the curvature and the local radius in 3D tissue can be more complex than in 2-dimen-

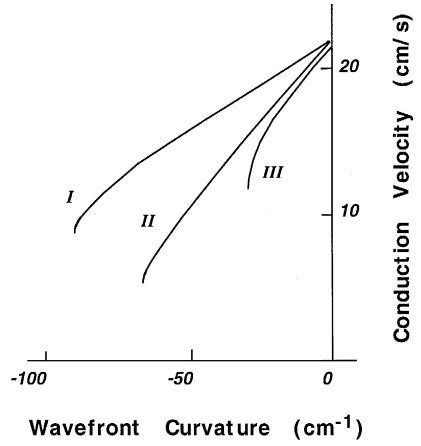

Fig. 2. Dependence of propagation velocity on wavefront curvature in several models of excitable media. I = Noble model [86]; II = Hramov and Krinsky model; III = Gul'ko and Petrov model [69]. Reproduced with permission [8].

sional (2D) tissue. For a cylindrical wavefront which is a 3D analogue of a circular wavefront, the relationship between the curvature and the local radius is the same as in the 2D medium ($\rho = -1/r$). For a sphere with radius r the local 3D curvature (ρ_{3D}) is:

$$\rho_{3D} = -\frac{2}{r} \tag{3}$$

It follows that the critical radius (r_c) in a 3D medium is 2 times larger than r_c in a 2D medium. Thus, the estimate for r_c of 152 μm in isotropic 2D cardiac tissue corresponds to 300 μm in 3D tissue. This difference reflects the fact that, for a given radius, the dissipation of excitatory current from a spherical 3D wavefront is larger than from the circular 2D wavefront.

2.3. Dependence of critical curvature on active and passive tissue properties

Eq. (2) allows one to predict how modulation of either passive or active tissue properties will affect the critical curvature. It follows from this equation that the effect of a change in membrane excitability on ρ_c is solely determined by the change of θ_0 and can, therefore, be estimated from experimental measurements of θ_0. For example, it is well known that conduction velocity decreases with high excitation rates. In atrial myocardium, velocity decreases approximately 2-fold in response to a very early premature stimulus or during pacing at the shortest possible interval [19]. According to Eq. (2), a 2-fold increase of the critical radius (r_c) is expected in these conditions. This frequency-dependent increase of r_c may be particularly important in tachycardias including flutter, or fibrillation.

According to Eq. (2), cell-to-cell coupling affects ρ_c and r_c via both the conduction velocity (θ_0) and the coefficient D. In a continuous uniform medium, the conduction velocity is inversely proportional to the square-root of intracellular resistivity R_i while the coefficient D is inversely proportional to R_i. It follows that ρ_c is inversely proportional to $R_i^{1/2}$. This dependence also allows one to evaluate the effect of anisotropy on critical curvature and critical radius. Thus, a wavefront propagating in the longitudinal direction has a critical radius of curvature which is $(R_T/R_L)^{1/2}$ times smaller than the r_c for a wavefront propagating in the transverse direction, where R_T and R_L are axial resistivities in longitudinal and transverse directions, respectively. Also, a circle of critical radius in an isotropic medium corresponds to an ellipse in an anisotropic medium with the transverse axis of this ellipse shortened by the factor $(R_T/R_L)^{1/2}$.

3. Occurrence of curved wavefronts in cardiac muscle

The estimates of critical curvature given above indicate that curvature effects are expected to become apparent in cardiac muscle when excitation fronts have bending radii $< 150–300$ μm. In cardiac tissue curved wavefronts with small radii are encountered in a variety of situations which include: (1) centrifugal propagation from a small stimulating electrode or from a small group of pacemaker cells; (2) abrupt changes in tissue geometry with propagation emerging from small narrow strands or isthmuses into a large mass of excitable tissue. Examples of such structures are Purkinje–muscle junctions, insertions of accessory pathways into ventricular muscle in the WPW syndrome, and probably surviving cell strands connecting regions of intact tissue in infarcted muscle; (3) propagation of a wave around a fixed anatomical or functional conduction block; (4) spiral wave rotation.

3.1. Wave propagation following point stimulation

Direct experimental evidence that wavefront curvature affects propagation of waves initiated from small stimulating electrodes was recently obtained by Knisley and Hill [20]. They investigated impulse conduction in 2-dimensional rims of epicardial tissue stimulated either by a single electrode or by a linear array of electrodes as shown in Fig. 3. Optical mapping of activation spread with a laser scanning technique demonstrated that stimulation with a single electrode resulted in an elliptic spread of excitation while stimulation with a linear array produced a nearly flat activation front. As a result of increased wavefront curvature, the velocity of the elliptical propagation was on the average 13% smaller than that of the flat wavefront. In these measurements, the spatially averaged velocity values were compared which underestimate the effect of steep wavefront curvature on local conduction velocity immediately near the stimulating electrode. Nevertheless, these data clearly demonstrate the importance of wavefront curvature. Measurements of conduction velocity as a function

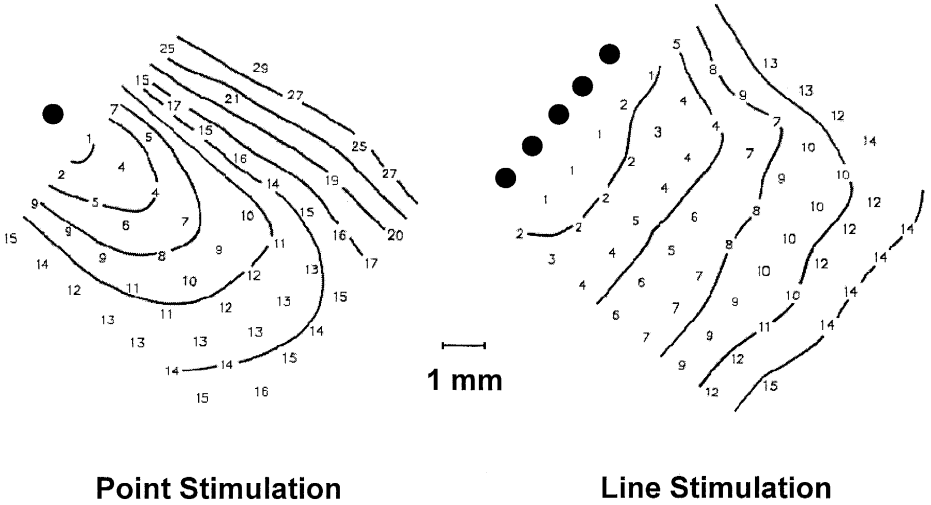

Fig. 3. Effect of point stimulation versus linear stimulations on activation spread. Stimulation with a single electrode (point stimulation) produces a convex excitation front. Stimulation with a line of electrodes (line stimulation) produces an almost flat excitation front. Numbers denote activation times in milliseconds relative to the earliest activation. Interval between isochrones is 3 ms. Reproduced with permission [20].

of curvature at small values of ρ were taken to determine the coefficient D in Eq. (1). The mean longitudinal D value was 0.47 cm^2/s. According to Eq. (2) this corresponds to a critical radius of 92 μm.

3.1.1. Wavefront curvature and 'liminal area'

The inability of excitable tissue to support propagation of waves with curvatures higher than ρ_c suggests that a critical number of cells encompassed within a nucleus of excitation with radius r_c must be excited to achieve a propagated response. A similar requirement has long been recognized for 1D excitable strands and formulated in the concept of 'liminal length' [21,22]. The 'liminal length' was defined as the length of an excited strand segment necessary to produce the local current required for a propagated response. Accordingly, in a 2D tissue this critical number of cells is characterized by a 'liminal area' [23]. Although the 'liminal area' of impulse initiation and a curved wavefront with a 'critical radius' may differ with respect to membrane potential distribution within the excited portion of the tissue, the common features between these processes can be used to estimate the 'critical radius' from the dimension of the 'liminal area', independently of the parameters D and θ_0 in Eq. (2).

The liminal area has been calculated in a 2-dimensional computer model by Ramza et al. [24]. They studied im-

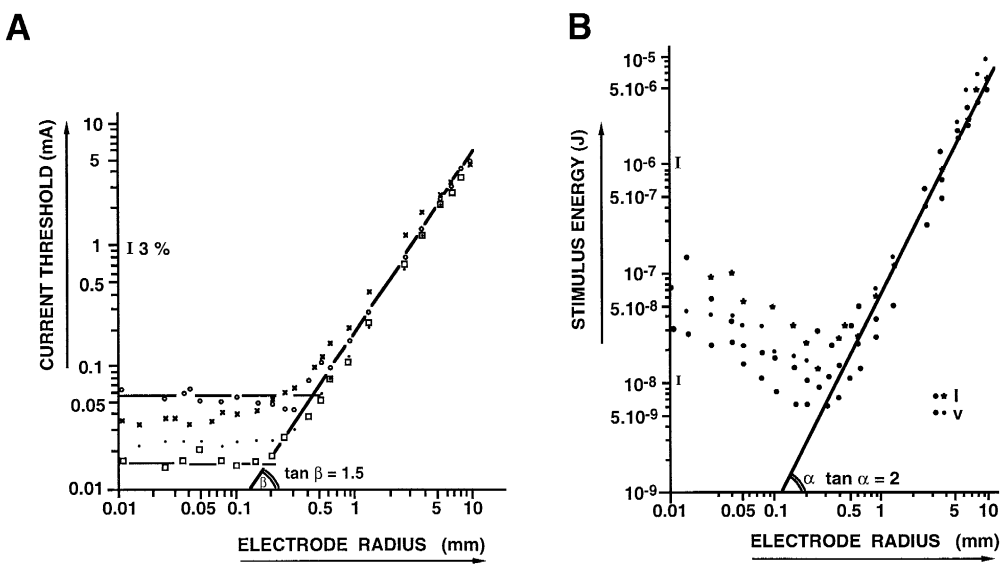

Fig. 4. Effect of the radius of a circular stimulation electrode on current threshold (A) and stimulus energy (B). Epicardial stimulation of canine heart. Reproduced with permission [23,26].

pulse initiation produced by a point current injection in a continuous, isotropic model described by Beeler-Reuter ionic kinetics [25]. The liminal area necessary to generate sufficient inward current during stimulation was determined as a function of the maximal sodium conductance. At a level of excitability estimated to correspond to that of adult ventricular myocardium, the radius of the liminal area was 200–250 μm. This compares well with the estimates of the critical radius calculated from Eq. (2). Experimentally, the liminal area was estimated from measurements of stimulation threshold as a function of electrode size by Lindemans and co-workers [23,26]. Stimulation current was applied to canine epicardium via disk electrodes with radii varying between 0.01 and 9 mm. As illustrated in Fig. 4A, it was found that the current threshold was independent of the electrode size when the disk radius was less than 0.2 mm. However, the current threshold was proportional to the electrode radius to the power 1.5 when the radius was larger than 0.4 mm. This behavior was explained by noting that, with small electrodes, all current passed through the liminal area and, therefore, current density at the edge of the liminal area was independent of the electrode size. With large electrodes, more current had to be provided to maintain a constant stimulatory current density as the electrode surface area increased. Thus, the estimated radius of the liminal area was approximately 0.3 mm. If we assume that the disk electrode excited a semi-spherical area of cardiac tissue under the epicardial surface, then this situation is equivalent to excitation of a spherical region in a tissue filling the whole 3D space. Therefore, the measured radius of the liminal area can be taken as an estimate of the critical radius of curvature. Scaled down from 3 to 2 dimensions, the estimated critical radius of 300 μm in the 3D tissue corresponds to 150 μm in the 2D tissue, which is close to the other estimates of the critical radius. Lindemans and Zimmerman [26] and Winfree [27] also pointed out a practical consequence of the 'liminal area' effect: an electrode with a radius matching the radius of liminal area is the most efficient (i.e., it requires the lowest stimulation energy, as illustrated in Fig. 4B).

3.2. Curved wavefronts at geometrical expansions

Abrupt geometrical expansions such as transitions from narrow strands to a large volume of myocardium or narrow isthmuses of tissue bridging two large areas of atrial or ventricular myocardium have been implicated in the formation of unidirectional conduction block and re-entry. Examples of such structures include the Purkinje–muscle junction [28], the junction between accessory pathways and myocardium in the WPW syndrome [29,30], and the junction between thin cell strands surviving within an infarcted myocardium and intact tissue [31,32]. The failure of impulse transmission at such structures was attributed to the 'impedance mismatch' between the strands and the wide

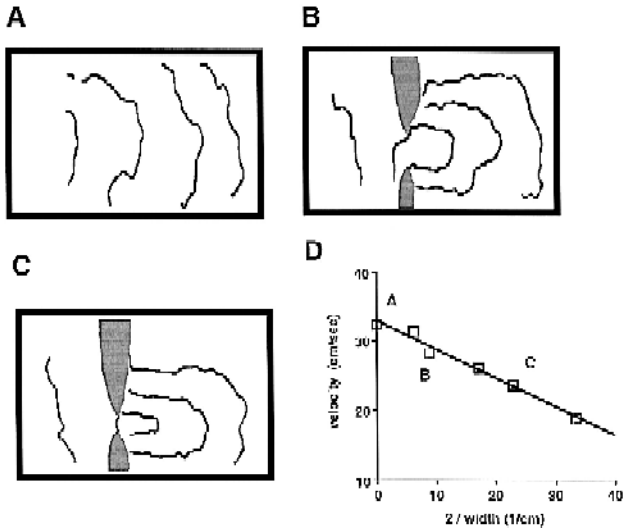

Fig. 5. Wave propagation across a narrow tissue isthmus in an isolated ventricular preparation of sheep heart. (A) Map of activation spread before an isthmus was produced. (B) Activation spread in the same preparation with isthmus 2.26 mm wide. The isthmus was produced by two tissue cuts (gray zones). (C) Activation spread after the isthmus was reduced to 0.88 mm. (D) Local conduction velocity measured across the isthmus as a function of isthmus width. Reproduced with permission [36].

tissue regions in analogy to conduction block in branching axons or cell strands [33–35]. More recently, however, a different approach was proposed which is based on consideration of the curvature of the wave front emerging from an expansion instead of the impedance mismatch at the transitional region. Cabo et al. [36] investigated impulse propagation across narrow isthmuses in isolated sheets of ventricular epicardial muscle using a video-imaging technique. As shown in Fig. 5, cuts were made in the preparations so that only a narrow isthmus of tissue (0.9–2.2 mm in width) bridging two large areas was left intact. The excitation wave emerging from such an isthmus had an elliptical shape with a pronounced curvature (panels B and C): the smaller the isthmus width, the higher the curvature of the elliptical wavefront beyond the isthmus. In accordance with the expected effect of increased curvature, conduction velocity in the region immediately beyond the isthmus decreased as the isthmus width became smaller (panel D). At the smallest isthmus shown in panel D the conduction velocity is 19 cm/s, 42% smaller than the velocity of the flat wave (33 cm/s). The critical radius, r_c, was estimated from the minimal isthmus width allowing passage of excitation waves between two large areas at various stimulation frequencies. At long cycle lengths (200 to 500 ms) the critical width was estimated to be < 1 mm in the longitudinal direction, corresponding to $r_c < 0.5$ mm. At a short excitation interval (150 ms) excitability was reduced and the critical isthmus width increased to 1.3–2 mm (critical radius 0.65–1 mm). At the maximal frequency of stimulation (117 ms interval) isthmuses with width < 2.5 mm ($r_c < 1.2$ mm) resulted in conduction block.

A similar expanding structure, consisting of a thin long strand emerging into a large tissue area, has been recently investigated both experimentally [37,38] and theoretically [39]. In computer simulations impulse propagation from a strand into a large area failed when the strand width was reduced below 200 μm in a 2D model or 350 μm in a 3D model. Fig. 6 illustrates the block of impulse propagation in the 2D model. The precise localization of the site of conduction block was obtained from the recordings of the excitatory inward sodium current (panel C). These recordings demonstrate that conduction block occurred *beyond* the site of geometrical expansion. A small circular nucleus of excitation emerged into the large area. Pronounced curvature of this nucleus imposed a large current drain on the wavefront and excitation did not propagate further. Experimentally, wave propagation from a narrow strand into a large cell area has also been investigated in cell cultures as a function of the strand width using high-resolution optical mapping of transmembrane potential [38]. In these studies, narrow myocyte strands emerging into a cell monolayer were produced using a patterned-growth technique [40]. As in simulations, wave propagation was either slowed or blocked when the strand width was reduced below a critical level. The critical strand width was approximately 30 μm. This is significantly smaller than the estimates of critical radius given above. This difference was explained by several geometrical and electrophysiological features of cell cultures: a shorter electrotonic space constant than in the adult myocardium, electrophysiological heterogeneity between the strands and the large areas, and a gradual increase of the strand width before the transition to the large area. When these properties were included into the computer model, a close fit between experimental and simulated results was obtained [39].

We would like to point out that the two approaches—the 'wavefront curvature' or 'impedance mismatch'—are related to the same biophysical mechanism: namely, the balance of electrical currents during wave propagation or the 'source–sink' relationship. The approach based on consideration of the wavefront curvature has an advantage of being able to relate, in a simple way, conduction block to electrophysiological parameters which can be directly measured in experiments (i.e., steady-state conduction velocity and passive tissue properties). Also, it helps to understand the occurrence of conduction block at an isthmus connecting two equal (i.e., symmetrical) areas where no impedance mismatch is present.

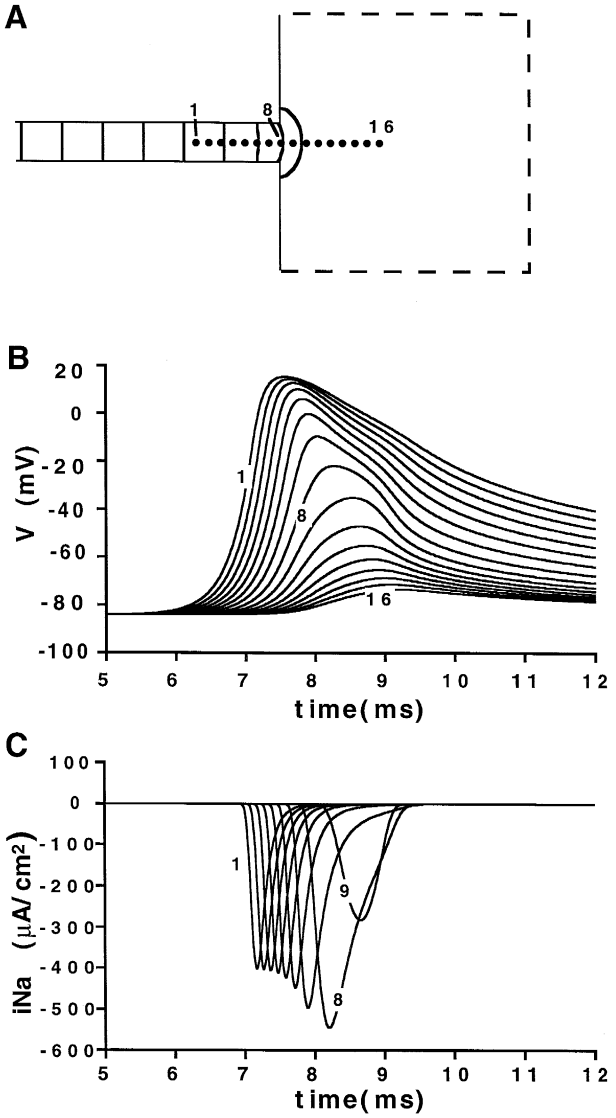

Fig. 6. Block of impulse propagation at a site of abrupt expansion from a narrow conducting strand into a large excitable area. Two-dimensional computer model with Luo-Rudy [43] ionic kinetics. Strand width = 175 μm. (A) Isochrone map of wave propagation with interval of 0.3 ms. (B and C) Recordings of membrane voltage (V) and inward sodium current (iNa) at the selected points depicted in panel A. Note that the depolarization wave invaded the large area creating a small circular nucleus of excitation. However, the excitation wave did not propagate beyond 100 μm from the expansion. Reproduced with permission [39].

3.3. Wavefront curvature and propagation around sharp obstacles

Sharp, longitudinally oriented obstacles, which may be structural or functional in nature, are thought to play an important role in so-called 'anisotropic re-entry' [41]. They have been described in the border zone of experimental infarcts and in the aging heart [41,42]. Computer simulations and recent experiments demonstrate that wavefront curvature has a profound effect on wave propagation near the sharp edges of such obstacles. Fig. 7 demonstrates wave propagation in a computer model of an excitable medium with a thin resistive obstacle. Ionic currents in this model are described by the Luo-Rudy kinetics [43] with maximal sodium conductance reduced to approximately 30% of its nominal value. As in Fig. 6, local activation is defined by the flow of sodium inward current. The refractory state is defined by inactivation of the sodium current. The isochronal activation map (panel A) demonstrates that

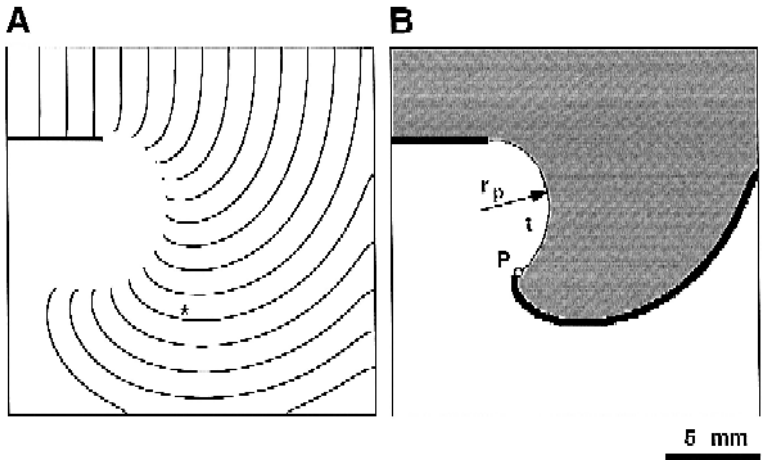

Fig. 7. Detachment of an excitation wave from the sharp edge of an unexcitable obstacle. Computer model with Luo-Rudy [43] ionic kinetics. The maximal sodium conductance was reduced to 6.6 mS/cm^2. (A) Isochronal map of activation spread with an interval of 5 ms. (B) Snapshot of activation at the moment marked by the asterisk in panel A. The black color shows the excited area defined by the activation of inward Na^+ current. The gray color shows the area in the refractory state as defined by Na^+ current inactivation. Point P marks the wave tip, defined as a point where excited, refractory, and resting states meet. The dashed line (t) shows the trajectory of the wave tip with the radius r_p.

as the propagation wave approaches the pivoting point, it detaches from the obstacle and describes a trajectory around a circular area which remains in the resting state. The detachment takes place since the critical curvature of the wavefront prohibits an abrupt turn around the sharp edge of the obstacle. Several electrophysiological features of this effect are of special importance not only for characterizing the process of propagation around unexcitable obstacles but also for describing the behavior of spiral waves in general (see below). As illustrated in Fig. 7B, there is a point on the wavefront (detached from the obstacle) where 3 states—the excited state (black), the refractory state (gray), and the resting state (white)—meet. We define this singular point as the tip of the wavefront. Accordingly, it is used to define the tip of a spiral wave and to describe spiral wave rotation (see below). The radius of the pivoting trajectory (r_p) is determined by the critical wavefront curvature or the critical radius, r_c. At present, the exact value of r_p in cardiac muscle is not known. The lack of detachment of a wave front from unexcitable obstacles in cardiac muscle under normal physiological conditions indicates that r_p is rather small (i.e., smaller than the spatial resolution of the mapping techniques which amounted to several hundred micrometers in these experiments) [44,45]. However, reduction of tissue excitability (e.g., by application of tetrodotoxin or by stimulation at high rates) increases r_c and r_p and causes detachment of wavefronts from a sharp obstacle [44]. Under conditions of very low excitability, the radius of the pivoting trajectory can become larger than the wavelength of excitation, the product of conduction velocity and refractory period. In this case, the wave may perform a complete turn without reconnecting to the obstacle and form a spiral wave. The detachment of excitation waves from sharp obstacles and subsequent formation of spiral waves was first described in a computer model at high excitation rates [46]; experimentally this has been observed in the chemical Belousov-Zhabotinsky reaction [47] and more recently in heart muscle [44].

4. Wavefront curvature and spiral waves

One of the most remarkable examples of wave propagation in which curvature plays an important role is a spiral wave of excitation. Spiral waves occur universally in excitable media including chemical reactions [48,49], neural tissue (depression waves in the retina [50] and cerebral cortex [51]), intracellular calcium signaling systems (*Xenopus laevis* oocytes [15], cardiac myocytes [52]), and amoebae colonies [53]. One of the most extensively studied examples is the Belousov-Zhabotinsky (BZ) reaction. In this reaction, malonic acid is reversibly oxidized by bromate in the presence of ferroin. In this process, ferroin changes in color from red to blue and then back to red, which allows the visual observation of the reaction. Fig. 8A shows a rotating spiral wave in a thin 2-dimensional layer of the BZ reaction. In the center of the rotating wave (core) the tip of the wave moves along a complex trajectory and radiates waves into the surrounding medium. Since the velocity of a convex wavefront cannot exceed the speed of the flat wave (θ_0) the rotating wave always acquires the shape of an Archimedean spiral at the periphery, *independently of the behavior of its core*. Because of this shape, rotating waves were given the name ‘spiral waves’. Other names used in the literature include ‘vortices’ and ‘reverberators’. In some cases, the term ‘rotor’ was used to refer to the core of a spiral wave.

Important properties of spiral waves including the rotation period, size, and dynamic behavior are determined by

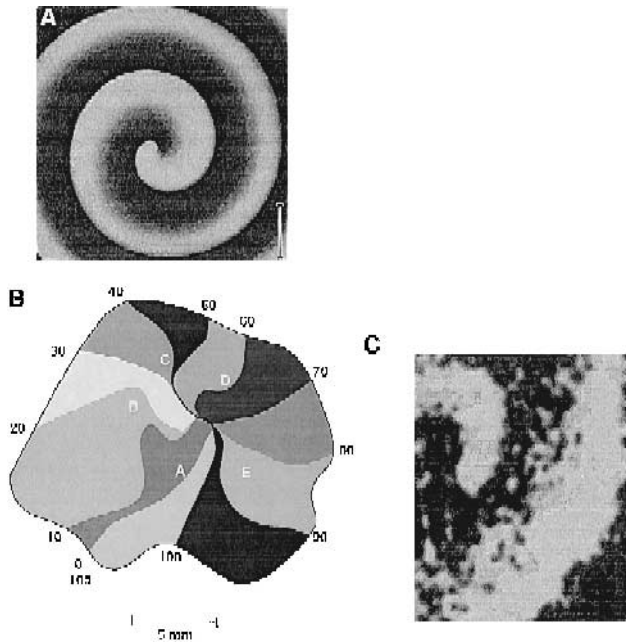

Fig. 8. Rotating waves in various excitable media. (A) Spiral wave in the Belousov-Zhabotinskii reaction. Reproduced with permission [49]. (B) Isochronal activation map of 'leading circle' re-entry in an isolated preparation of rabbit atrial muscle. Reproduced with permission [64]. (C) Spiral wave in an isolated preparation of canine epicardial muscle imaged using voltage-sensitive dye. Reproduced with permission [71].

the wave propagation in the core where the wavefront has a pronounced curvature. The theory of excitable waves suggests that two factors—the wavefront curvature and the refractory period—contribute to the period of spiral wave rotation [6,10]. Mutual dependence and interaction between these parameters result in a complex behavior of spiral waves. Because of this complexity, the understanding of spiral wave dynamics relies heavily on computer modeling. A convenient way to relate the behavior of spiral waves with model parameters is to use cellular automata models of cardiac excitation. In such models, excitable elements are described by 4 states (excited, absolute refractory, relative refractory, and resting) and the transition from one state to another is governed by formal rules [54]. One of the advantages of these models is that integrative properties of excitable media such as excitability and the durations of the absolute and relative refractory periods are set as model parameters and can be modified independently. Importantly, these models can be constructed to reproduce the effects of wave front curvature on conduction velocity. Although cellular automata models oversimplify active and passive properties of cardiac tissue, they provide an easy insight into spiral wave dynamics.

4.1. Curvature and spiral wave dynamics

Fig. 9 demonstrates 3 different types of spiral wave rotation in a cellular automata model of excitable medium [55]. As in Fig. 7, the wavefront tip is defined as the point where 3 states—the excited, the refractory, and the resting—are in contact with each other. Fig. 9A shows the simplest type of spiral wave rotation when the excitability in the model is very low. In this case, the critical radius (r_c) and therefore the pivoting radius of the wave tip (r_p) are large. By contrast, the wavelength of excitation (λ) given by the product of the velocity of propagation (θ) and the refractory period [R, ($\lambda = \theta * R$)] is small as a result of the small θ. Under these conditions the length of the pivoting trajectory ($2\pi r_p$) is larger than λ, and therefore propagation of the excitation wavefront is not affected by the refractory tail. The only constraint on the wavefront propagation is imposed by the curvature at its tip. Because the wavefront curvature cannot exceed the critical curvature (ρ_c) the wave tip does not extend towards the center of the rotation but follows a circular trajectory (panel A, bottom). The area circumscribed by the circle is never excited and remains at rest. In addition, there is a zone in the resting state between the wave front and the wave tail. In other words, the spiral wave contains a fully excitable gap.

At a higher level of excitability, when r_p decreases and the length of the pivoting trajectory becomes comparable with the wavelength of excitation ($2\pi r_p \approx \lambda$), the front of the excitation wave meets its own refractory tail, as shown in Fig. 9B. As a result, the wavefront velocity decreases and the front retreats from the refractory tail. It now propagates in a fully recovered medium and the velocity increases again. The alternation of wavefront acceleration and retardation repeats itself in a complex dynamic manner. Such a front–tail interaction results in a 'meandering' of the spiral wave tip as shown at the bottom of panel B. The movement of the wave tip in this case follows a cycloidal or 'flower' trajectory. Such a meandering movement of spiral waves was observed in the BZ reaction

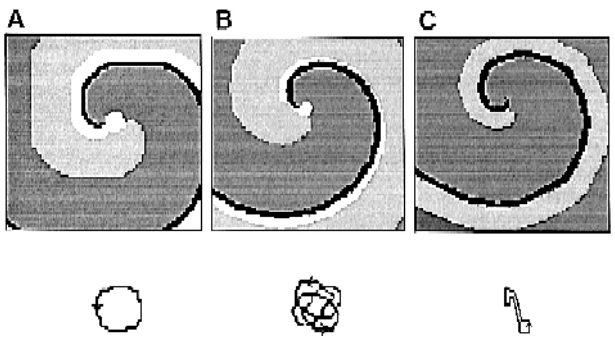

Fig. 9. Effect of wavefront curvature on spiral wave rotation in a cellular automata model of an excitable medium. Upper panels show snapshots of activation. Excited, absolute refractory, relative refractory, and resting states are shown in black, dark gray, light gray, and white, respectively. Lower panels show enlarged trajectories of the spiral wave tip. (A) Circular type of rotation in a model with large critical curvature ($2\pi r_p > \lambda$). (B) Cycloidal type of rotation in a model with intermediate level of critical curvature ($\lambda \approx 2\pi r_p$). (C) 'Z' type of rotation in a model with small critical curvature ($\lambda > 2\pi r_p$). Reproduced with permission [55].

[5,56] and was extensively investigated in a variety of mathematical models [6,55,57–63].

With a further increase of wavelength relative to the pivoting radius ($\lambda > 2\pi r_p$) the interaction between the wave front and the partially refractory wave tail becomes stronger. Fig. 9C shows that, in this case, the wavefront penetrates deeper into the wave tail and there is no fully excitable gap. A part of the wave tip trajectory acquires a linear shape. The linear part is formed when the tip of the spiral wave moves along its refractory tail, which serves as a zone of functional conduction block. At the end of the line of the block, the wave tip performs a turn and propagates in the opposite direction. As a result, the wave tip trajectory is composed of the linear portion and two circular parts at the ends of the linear portion arranged as a letter 'Z', as shown in the lower part of panel C. The size of the circular parts in such a trajectory depends on the pivoting radius (r_p). The length of the linear portion depends on the wavelength of excitation. Therefore, an increase in the ratio λ/r_p increases the linear part of the trajectory and decreases the circular part. In the extreme case of a negligibly small r_p, the propagation of the excitation front depends only on the state of recovery in the tissue ahead of the wavefront. Consequently, the separation between the front and the absolute refractory tail is determined by the driving force of the wavefront moving within the relative refractory period. In this case the mechanism of spiral wave rotation is similar to the mechanism postulated in the so-called 'leading circle' concept [64].

The types of spiral wave rotation described by the cellular automata model in Fig. 9 are also observed in computer models based on partial differential equations (FitzHugh-Nagumo model [60] and Beeler-Reuter model [61]). Fig. 10 shows trajectories of the spiral wave tip in the FitzHugh-Nagumo model upon increasing the wavelength of excitation (λ), while the pivoting radius (r_p) remains constant [60]. As in the cellular automata model (Fig. 9), spiral wave rotation changes from circular to cycloidal, and then to 'Z' type as the ratio between λ and r_p increases. Interestingly, the rotation of spiral waves in the computer simulations shown in Figs. 9 and 10 is never stable, except for the extreme case of circular rotation

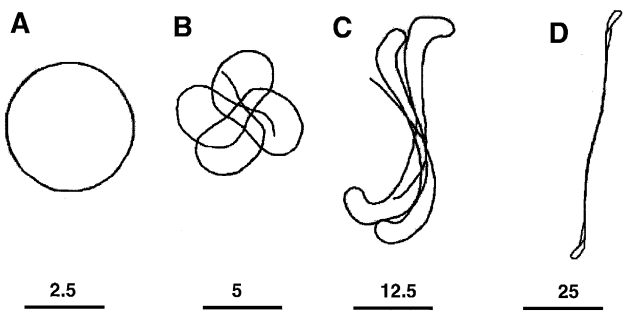

Fig. 10. Trajectories of the spiral wave tip of circular (A), cycloidal (B), and 'Z' types (C and D) of rotation in the FitzHugh-Nagumo model. Bars at the bottom show relative scaling. Reproduced with permission [60].

when the length of the pivoting trajectory is larger than λ. The strongest meandering is observed at intermediate levels of the ratio λ/r_p. Such meandering of spiral wave rotation has been implicated in the generation of polymorphic ECG's related to cardiac arrhythmias such as *torsades de pointes* [62,65]. With high values of λ/r_p the linear zone of functional conduction block also moves, although more slowly.

The results presented above were obtained in isotropic models. They can be directly extended to anisotropic tissue with continuous electrical properties. In such a case, the effect of changing anisotropic tissue ratio is equivalent to geometrical scaling in the transverse direction by a factor which equals the square root of the ratio between resistivities in transverse and longitudinal directions. Introducing anisotropy in such a way does not change the period of spiral wave rotation or the duration of excitable gap [66].

4.2. Occurrence of spiral waves in cardiac muscle

In the heart, spiral waves have long been implicated in the generation of cardiac arrhythmias [48,67–69]. However, the first experimental observation of rotating waves in atrial muscle [70] and later mapping studies in a variety of preparations revealed a pattern of activation spread that differed in part from the spiral shape (Fig. 8B). Thus, the isochrone lines were only slightly bent and deviated from the spiral shape shown in Fig. 8A. There are two possible explanations for this discrepancy: (1) Only the central portion of the wave near its tip was observed in a tissue approximately 2 cm in diameter and, therefore, the spiral shape was less prominent. (2) The spiral shape might have been further masked by electrophysiological heterogeneities present in atrial muscle. However, provided that the size of the preparation is large and/or the excitation wavelength is small, the wavefront will inevitably acquire a spiral shape. Indeed, in preparations with short excitation wavelength (low excitability and/or low degree of cellular coupling), rotating waves show a distinct spiral shape (Fig. 8C) [71].

As described above (Figs. 9 and 10), the type of rotation (i.e., the trajectory followed by the spiral wave tip) is determined by the relation between the excitation wavelength (λ) and the pivoting radius (r_p). The wavelength of excitation during sustained rotation is well known and amounts to approximately 3 cm (a velocity of 30 cm/s times an absolute refractory period of 0.1 s). The value of the pivoting radius in cardiac muscle has not been measured yet. As discussed above, it is very small at normal excitability, perhaps in the range of several hundred micrometers. Thus, λ is significantly larger than the estimated value of the pivoting radius in the normal case. Therefore, for cardiac tissue in a normal state of cell-to-cell coupling and with normal excitability, the trajectory of the tip is expected to assume the linear or Z-type of shape shown in Fig. 9C and 10D. This theoretical consideration

is supported by experimental observation from mapping experiments showing that the zone of functional conduction block often has a linear shape [19,72,73]. The linear trajectory of the rotating wave tip is also seen in the work of Allessie et al. (Fig. 3 of Ref. [64]). Under conditions of reduced excitability spiral waves with cycloidal or even circular types of rotation (Fig. 9A and 10A) can be anticipated.

4.3. Wavefront curvature and drift of spiral waves

In addition to meandering in the center of a spiral wave, spiral wave instability may involve drift due to the electrophysiological heterogeneity of cardiac tissue. The first experimental observation of spiral wave drift in cardiac muscle was reported by Fast and Pertsov [74]. In this work, spiral waves were initiated in isolated 2-dimensional preparations of rabbit ventricular epicardium. Preparations were placed in a chamber with two compartments divided by a thin rubber barrier. A functional heterogeneity in refractoriness and conduction velocity was created by separate superfusion of two compartments with normal versus quinidine-containing solutions. As shown in Fig. 11, premature stimulation from the area with the low refractoriness induced a conduction block at the border between the two compartments (panel A) and the formation of a spiral wave rotating in a counterclockwise direction. On subsequent cycles (panel B) the spiral wave moved along the border of heterogeneity (perpendicular to the gradient of refractoriness) and continued to drift until it died at the border of the preparation (panel C). The drift velocity amounted to about one-fifth of the propagation velocity, and its direction was determined by the direction of wave rotation and the gradient of refractoriness. When a spiral wave with a clockwise rotation was initiated, it drifted in the opposite direction.

Due to the drift of a spiral wave, the frequency of excitation at a given measurement site depends on the location of this site relative to the moving spiral. This effect is known in the theory of electromagnetic and acoustic waves as the *Doppler effect*. Fig. 11D shows excitation intervals measured during spiral wave drift at different tissue locations. The measuring sites were distributed along the boundary of heterogeneity which determined the direction of the drift. Because of the drift, the sites located in front of the drifting spiral wave were excited significantly faster than the sites located behind it. The difference in excitation intervals measured ahead of and behind the spiral wave amounted to 30%. Drift of spiral waves and the Doppler effect were also observed in isolated preparations of sheep ventricular muscle imaged with an optical mapping technique [66,71]. In this case, no artificial heterogeneity was created and the spiral wave drift was likely to be a result of intrinsic spatial gradients of electrophysiological properties. The Doppler effect and the coexistence of different excitation frequencies within

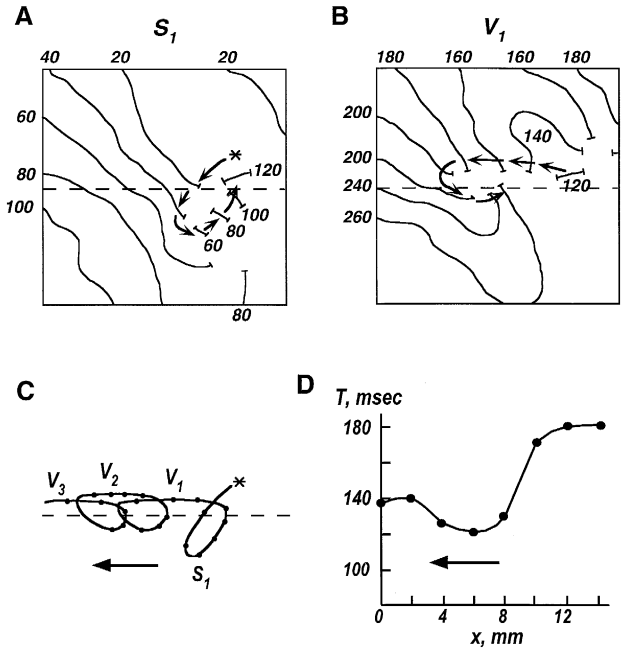

Fig. 11. Drift of a spiral wave and the Doppler effect. (A and B) Isochronal activation maps showing initiation (A) and the first rotation cycle (B) of a spiral wave in an isolated preparation of epicardial muscle. A stepwise inhomogeneity in refractory period was created by separate superfusion of two parts of the preparation with normal and quinidine-containing solutions. Dashed line shows the border of inhomogeneity with smaller refractoriness in the upper part. The asterisk shows the location of the stimulation electrode. (C) Trajectory of the spiral wave tip during initiation (S_1) and 3 subsequent cycles of spiral wave rotation (V_1–V_3). (D) Excitation intervals measured along the border of inhomogeneity during spiral wave drift (cycle V_2). Because of the drift, excitation intervals in front of the spiral wave are significantly shorter than intervals behind the spiral wave (Doppler effect). Reproduced with permission [74].

the same preparation have been used to explain a possible mechanism of the ECG pattern observed during arrhythmias (*torsades de pointes* [66,75]).

Theoretical analysis of the drift mechanism in mathematical models has demonstrated that, similarly to spiral wave meandering, the drift is strongly dependent on the relationship between the wavelength of excitation and the critical radius of curvature. Depending on the λ/r_p ratio, two different mechanisms of spiral wave drift can be distinguished. In one extreme situation when λ is much larger than r_p, spiral wave rotation is mainly determined by the tissue refractory period. In this case, the drift of spiral waves is governed by spatial gradients in refractoriness [54,76]. Accordingly, in a medium with a stepwise heterogeneity, spiral waves drift along the borders separating regions with different refractoriness as shown in Fig. 11. With an increase in r_p and/or a decrease in λ the drift is influenced by a new component: in addition to drifting along the boundary, the spiral wave shifts into the region with the larger rotation periods. In the extreme case of $2\pi r_p \gg \lambda$, the spiral wave rotation is no longer affected by refractoriness and the drift is governed by local gradi-

ents in r_p alone. In the case of a stepwise gradient in r_p, the drift is directed predominantly along the border separating regions with different r_p [77,78], similar to the case of purely refractoriness-dependent drift.

4.4. Stationary spiral waves, anchoring effect

In many of the experimentally-induced tachycardias, the initial transition from a normal propagation pattern during a basic beat to a rotating pattern is caused by a premature wave propagating through tissue with heterogeneous refractoriness. According to the mechanism of spiral wave instability described above, such waves should be unstable due to refractoriness-dependent drift. However, mapping experiments have shown that such waves are often stable, rotating rigidly around a fixed core [41,73]. This discrepancy can be explained by the stabilizing effects of small localized discontinuities in tissue structure corresponding to unexcitable obstacles [71]. Fig. 12 shows an example of the anchoring of an initially drifting spiral wave [79]. Electrical activity in this case is represented in the form of a time–space plot (panel B) where signals from all measuring points were compressed into a single line which is displayed as a function of time (see Ref. [71] for details). In such diagrams, a propagating wave is represented by a narrow band and the location of the spiral wave core is equivalent to the point of band branching. Initially the spiral wave drifted in a downward direction as shown by the straight line. After 8 cycles of rotation, the spiral wave was anchored and became stationary. In most cases of stable rotation a band of connective tissue or a small branch of the coronary artery was identified as the site of anchoring.

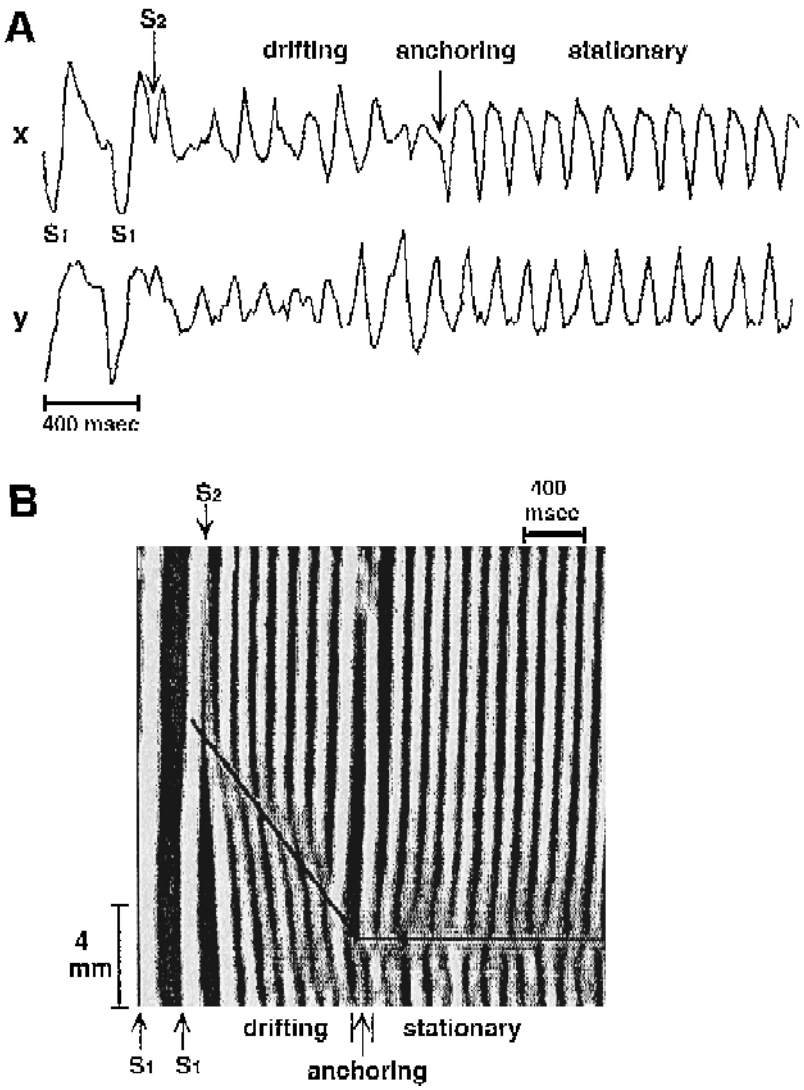

Fig. 12. Anchoring of a drifting spiral wave. (A) Electrocardiographic recordings showing that premature stimulation (S_2) produced polymorphic arrhythmic activity followed by a transition to sustained monomorphic tachycardia. (B) Time–space plot of activation spread obtained from video-imaging of the fluorescence of a voltage-sensitive dye. In these plots activity from the whole image is projected onto a single direction (vertical axis) and displayed as a function of time. White bands show planar wave propagation while the branching of bands indicates the presence of a spiral wave induced by S_2 stimulation. The spiral wave drifted during the first 7 cycles and became stationary thereafter. Reproduced with permission [79].

The anchoring of spiral waves by unexcitable obstacles depends on the relation between the critical radius of curvature (r_c) and the size and shape of the obstacle. The smaller the r_c, the stronger the interaction between the spiral wave tip and the obstacle. As a result, anchoring of spiral waves is more likely to occur in conditions of relatively high excitability. In a medium with large r_c, excitation waves tend to detach from sharp obstacles (Fig. 7), and therefore obstacles are less likely to anchor spiral waves.

4.5. Spiral waves in 3 dimensions

Representation of myocardium as a 2-dimensional excitable medium is valid in a case of relatively thin myocardial tissue such as atrial muscle [64] or a thin layer of epicardium surviving after myocardial infarction [41] or the cryo-ablation procedure [80]. However, in other cases such as a left ventricular wall, the 3-dimensional structure of cardiac muscle must be taken into account. Analogues of spiral waves in 3 dimensions are called 'scroll waves'. A spiral wave core in a 2-dimensional medium corresponds to a filament in a 3-dimensional medium around which rotation of a scroll wave occurs. The simplest case of a scroll wave is an extension of a 2-dimensional spiral wave into the third dimension. Provided that cardiac tissue is homogeneous and the scroll filament is a straight line, the behavior of such a wave is equivalent to the behavior of a 2-dimensional spiral wave. The behavior of a scroll wave may become different when muscle properties vary with depth or when the scroll wave filament is bent or twisted. The specific 3-dimensional effects related to scroll wave rotation were quite extensively investigated in computer models. A brief review of these data has been published recently [81]. One of the interesting effects specific to the 3-dimensional media is the unstable rotation of scroll waves with filaments which are bent or closed into rings [82]. The mechanism for such instability relates to the 3-dimensional wavefront curvature, which may occur even if the rotation of a corresponding 2-dimensional spiral wave is stable and which may result in termination of the scroll wave. Another intriguing theoretical possibility is a persistent but disordered rotation of a scroll wave in homogenous 3-dimensional media resulting in a fibrillation-like electrical activity when projected to a surface of the medium [83]. The experimental verification of these effects in cardiac muscle is still lacking due to the inability to map 3-dimensional activation spread with sufficiently high spatial resolution.

4.6. Concluding remarks

In summary, the experimental and theoretical data available at present clearly demonstrate the importance of the wavefront geometry in cardiac impulse propagation and in the behavior of spiral waves. Critical wavefront curvature contributes to a number of physiologically relevant effects: (1) conduction block at structures with abrupt tissue isthmuses or expansions; (2) dependence of stimulation strength on electrode size; (3) formation of an excitable gap during spiral wave rotation; (4) meandering, drift and anchoring of spiral waves. The application of theory based on continuous model to cardiac muscle in a quantitative way may have limitations, especially taking into account the fact that the estimated value of the critical radius is comparable to the dimensions of an individual cardiac cell. However, the fact that the value of critical curvature predicted from the theory and from the computer simulations in continuous models is close to the experimental estimates suggests that the continuous model is a good approximation, at least for healthy tissue. That may be different in aging tissue and in pathological conditions such as infarction and hypertrophy where larger discontinuities in axial resistivity may be present. Another limitation of the present approach is that it does not take into account the extracellular space. It is well established that impulse initiation and propagation in a tissue with a restricted extracellular space are strongly affected by differences in the anisotropic resistivity ratio between intra- and extracellular spaces as described by bi-domain models [84,85]. The extent to which these factors affect critical curvature remains unknown.

Acknowledgements

We wish to thank Dr. Hans Peter Clamann and Dr. John Shiner for reading this manuscript, Mrs. Lilly Lehmann for help in preparation of figures. This work was supported by the Swiss National Science Foundation and the Swiss Heart Foundation.

References

[1] Jack JJB, Noble D, Tsien RW. Electric Current Flow in Excitable Cells. Oxford: Clarendon Press, 1975.
[2] Spach MS, Kootsey JM. The nature of electrical propagation in cardiac muscle. Am J Physiol 1983;244:H3–H22.
[3] Janse MJ. Reentrant arrhythmias. In: HA Fozzard, eds. The Heart and Cardiovascular System. New York: Raven Press, 1992;2055–2094.
[4] Rudy Y. Models of continuous and discontinuous propagation in cardiac tissue. In: Zipes DB, Jalife J, eds. Cardiac Electrophysiology. From Cell to Bedside. Philadelphia: Saunders, 1995;326–334.
[5] Winfree AT. When Time Breaks Down. Princeton: Princeton University Press, 1987.
[6] Zykov VS. Simulation of Wave Processes in Excitable Media. Manchester: Manchester University Press, 1987.
[7] Keener JP. A geometrical theory for spiral waves in excitable media. SIAM J Appl Math 1986;46:1039–1056.
[8] Zykov VS, Morozova OL. Speed of spread of excitation in two-dimensional excitable medium. Biophysics 1979;24:739–744.
[9] Zykov VS. Analytical evaluation of the dependence of the speed of an excitation wave in a two-dimensional excitable medium on the curvature of its front. Biophysics 1980;25:906–911.
[10] Tyson JJ, Keener JP. Singular perturbation theory of traveling waves in excitable media. Physica D 1988;32:327–361.

[11] Gerhardt M, Schuster H, Tyson JJ. A cellular automaton model of excitable media including curvature and dispersion. Science 1990;247:1563–1566.
[12] Sneyd J, Atri A. Curvature dependence of a model for calcium wave propagation. Physica D 1993;65:365–372.
[13] Foerster P, Muller SC, Hess B. Curvature and propagation velocity of chemical waves. Science 1988;241:685–687.
[14] Foerster P, Muller SC, Hess B. Critical size and curvature of wave formation in an excitable medium. Proc Natl Acad Sci USA 1989;86:6831–6834.
[15] Lechleiter J, Girard S, Peralta E, Clapham D. Spiral calcium wave propagation and annihilation in Xenopus laevis oocytes. Science 1991;252:123–126.
[16] Clerc L. Directional differences of impulse spread in trabecular muscle from mammalian heart. J Physiol (Lond) 1976;255:335–346.
[17] Spach MS, Heidlage JF. The stochastic nature of cardiac propagation at a microscopic level—electrical description of myocardial architecture and its application to conduction. Circ Res 1995;76:366–380.
[18] Kléber AG, Riegger CB, Janse MJ. Electrical uncoupling and increase of extracellular resistance after induction of ischemia in isolated, arterially perfused rabbit papillary muscle. Circ Res 1987;61:271–279.
[19] Smeets JLRM, Allessie MA, Lamers WJEP, Bonke FIM, Hollen J. The wavelength of the cardiac impulse and reentrant arrhythmias in isolated rabbit atrium. The role of heart rate, autonomic transmitters, temperature, and potassium. Circ Res 1986;58:96–108.
[20] Knisley SB, Hill BC. Effects of bipolar point and line stimulation in anisotropic rabbit epicardium. assessment of the critical radius of curvature for longitudinal block. IEEE Trans Biomed Eng 1995;42:957–966.
[21] Noble D. The relation of Rushton 'liminal length' for excitation to the resting and active conductances of excitable cells. J Physiol 1972;226:573–591.
[22] Fozzard HA, Schoenberg M. Strength–duration curves in cardiac Purkinje fibres. effects of liminal length and charge distribution. J Physiol 1972;226:593–618.
[23] Lindemans FW, van der Gon JJD. Current thresholds and liminal size in excitations of heart muscle. Cardiovasc Res 1978;12:477–485.
[24] Ramza BM, Joyner RW, Tan RC, Osaka T. Cellular mechanism of the functional refractory period in ventricular muscle. Circ Res 1990;66:147–162.
[25] Beeler GW, Reuter H. Reconstruction of the action potential of ventricular myocardial fibres. J Physiol 1977;268:177–210.
[26] Lindemans FW, Zimmerman ANE. Acute voltage, charge, and energy thresholds as functions of electrode size for electrical stimulation of the canine heart. Cardiovasc Res 1979;13:383–391.
[27] Winfree AT. The electrical thresholds of ventricular myocardium. J Cardiovasc Electrophysiol 1990;1:393–410.
[28] Mendez C, Mueller WJ, Merideth J, Moe GK. Interaction of transmembrane potentials in canine Purkinje fibers and at Purkinje fiber–muscle junctions. Circ Res 1969;34:361–372.
[29] De la Fuente D, Sasyniuk B, Moe GK. Conduction through a narrow isthmus in isolated canine atrial tissue. A model of the W-P-W syndrome. Circulation 1971;44:803–809.
[30] Inoue H, Zipes DP. Conduction over an isthmus of atrial myocardium in vivo. a possible model of Wolf-Parkinson-White syndrome. Circulation 1987;76:637–647.
[31] Smith JH, Green CR, Peters NS, Rothery S, Severs NJ. Altered patterns of gap junction distribution in ischemic heart disease—an immunohistochemical study of human myocardium using laser scanning confocal microscopy. Am J Pathol 1991;139:801–821.
[32] De Bakker JMT, Van Capelle FJL, Janse MJ, et al. Slow conduction in the infarcted human heart—zigzag course of activation. Circulation 1993;88:915–926.
[33] Khodorov BI, Timin YN, Vilenkin SY, Gul'ko FB. Theoretical analysis of the mechanisms of conduction of a nerve pulse over an inhomogeneous axon. I. Conduction through a portion with increased diameter. Biofizika 1969;14:304–315.
[34] Goldstein SS, Rall W. Changes of action potential shape and velocity for changing core conductor geometry. Biophys J 1974;14:731–757.
[35] Joyner RW, Veenstra R, Rawling D, Chorro A. Propagation through electrically coupled cells. Effects of a resistive barrier. Biophys J 1984;45:1017–1025.
[36] Cabo C, Pertsov AM, Baxter WT, Davidenko JM, Gray RA, Jalife J. Wave-front curvature as a cause of slow conduction and block in isolated cardiac muscle. Circ Res 1994;75:1014–1028.
[37] Rohr S, Salzberg BM. Characterization of impulse propagation at the microscopic level across geometrically defined expansions of excitable tissue. multiple site optical recording of transmembrane voltage (MSORTV) in patterned growth heart cell cultures. J Gen Physiol 1994;104:287–309.
[38] Fast VG, Kléber AG. Cardiac tissue geometry as a determinant of unidirectional conduction block. assessment of microscopic excitation spread by optical mapping in patterned cell cultures and in a computer model. Cardiovasc Res 1995;29:697–707.
[39] Fast VG, Kléber AG. Block of impulse propagation at an abrupt tissue expansion. evaluation of the critical strand diameter in 2- and 3-dimensional computer models. Cardiovasc Res 1995;30:449–459.
[40] Rohr S, Schölly DM, Kléber AG. Patterned growth of neonatal rat heart cells in culture. Morphological and electrophysiological characterization. Circ Res 1991;68:114–130.
[41] Wit AL, Dillon SM. Anisotropic reentry. In: DP Zipes, Jalife J, eds. Cardiac Electrophysiology. From Cell to Bedside. Philadelphia: Saunders, 1990;353–364.
[42] Spach MS, Dolber PC. Relating extracellular potentials and their derivatives to anisotropic propagation at a microscopic level in human cardiac muscle. Evidence for electrical uncoupling of side-to-side fiber connections with increasing age. Circ Res 1986;58:356–371.
[43] Luo CH, Rudy Y. A model of the ventricular cardiac action potential—depolarization, repolarization, and their interaction. Circ Res 1991;68:1501–1526.
[44] Cabo C, Pertsov AM, Davidenko JM, Baxter WT, Gray RA, Jalife J. Vortex shedding as a result of turbulent electrical activity in cardiac muscle. Biophys J 1996;70:1105–1111.
[45] Girouard SD, Pastore JM, Laurita KR, Gregory KW, Rosenbaum DS. Optical mapping in a new guinea pig model of ventricular tachycardia reveals mechanisms for multiple wavelengths in a single reentrant circuit. Circulation 1996;93:603–613.
[46] Pertsov AM, Panfilov AV, Medvedeva FU. Instabilities of autowaves in excitable media associated with critical curvature phenomenon. Biofizika 1983;28:100–102.
[47] Agladze K, Keener JP, Muller SC, Panfilov A. Rotating spiral waves created by geometry. Science 1994;264:1746–1748.
[48] Winfree AT. Spiral waves of chemical activity. Science 1972;175:634–636.
[49] Müller SC, Plesser T, Hess B. The structure of the core of the spiral wave in the Belousov-Zhabotinskii reaction. Science 1985;230:661–663.
[50] Gorelova NA, Bures J. Spiral waves of spreading depression in the isolated chicken retina. J Neurobiol 1983;14:353–363.
[51] Shibata J, Bures J. Optimum topographical conditions for reverberating cortical spreading depression in rats. J Neurobiol 1974;5:107–118.
[52] Lipp P, Niggli E. Microscopic spiral waves reveal positive feedback in subcellular calcium signaling. Biophys J 1993;65:2272–2276.
[53] Tomchik KJ, Devreotes PN. Adenosine 3′,5′-monophosphate waves in Dictyostelium discoideum. a demonstration by isotope dilution-fluorography. Science 1981;212:443–446.
[54] Fast VG, Efimov IR. Stability of vortex rotation in an excitable cellular medium. Physica D 1991;49:75–81.
[55] Fast VG, Efimov IR, Krinsky VI. Transition from circular to linear

rotation of a vortex in an excitable cellular medium. Phys Lett A 1990;151:157–161.
[56] Winfree AT. Scroll-shaped waves of chemical activity in three dimensions. Science 1973;181:937–939.
[57] Zykov VS. Cycloid circulation of spiral waves in excitable medium. Biophysics 1986;31:940–944.
[58] Lugosi E. Analysis of meandering in Zykov kinetics. Physica D 1989;40:331–337.
[59] Gerhardt M, Schuster H, Tyson JJ. A cellular automaton model of excitable media. II. Curvature, dispersion, rotating waves and meandering waves. Physica D 1990;46:392–415.
[60] Krinsky VI, Efimov IR, Jalife J. Vortices with linear cores in excitable media. Proc Roy Soc London Ser A 1992;437:645–655.
[61] Efimov I, Krinsky V, Jalife J. Dynamics of rotating vortices in the Beeler-Reuter model of cardiac tissue. Chaos, Solitons and Fractals 1995;5:513–526.
[62] Starmer CF, Romashko DN, Reddy RS, et al. Proarrhythmic response to potassium channel blockade. numerical studies of polymorphic tachyarrhythmias. Circulation 1995;92:595–605.
[63] Holden AV, Zhang H. Characteristics of atrial re-entry and meander computed from a model of a rabbit single atrial cell. J Theor Biol 1995;175:545–551.
[64] Allessie MA, Bonke FIM, Schopman FJC. Circus movement in rabbit atrial muscle as a mechanism of tachycardia. III. The ‘leading circle’ concept. a new model of circus movement in cardiac tissue without the involvement of an anatomical obstacle. Circ Res 1977;41:9–18.
[65] Gray RA, Jalife J, Panfilov A, et al. Nonstationary vortexlike reentrant activity as a mechanism of polymorphic ventricular tachycardia in the isolated rabbit heart. Circulation 1995;91:2454–2469.
[66] Pertsov AM, Davidenko JM, Salomonsz R, Baxter WT, Jalife J. Spiral waves of excitation underlie reentrant activity in isolated cardiac muscle. Circ Res 1993;72:631–650.
[67] Selfridge O. Studies of flutter and fibrillation. Arch Inst Cardiol Mexico 1948;18:177–187.
[68] Balakhovsky IS. Several modes of excitation movement in ideal excitable tissue. Biophysics 1965;10:1175–1179.
[69] Gul’ko FB, Petrov AA. Mechanism of the formation of closed pathways of conduction in excitable media. Biophysics 1972;17:271–282.
[70] Allessie MA, Bonke FIM, Schopman FJC. Circus movement in rabbit atrial muscle as a mechanism of tachycardia. Circ Res 1973;33:54–62.
[71] Davidenko JM, Pertsov AV, Salomonsz R, Baxter W, Jalife J. Stationary and drifting spiral waves of excitation in isolated cardiac muscle. Nature 1992;355:349–351.
[72] Frazier DW, Wolf PD, Wharton JM, Tang ASL, Smith WM, Ideker RE. Stimulus-induced critical point. Mechanism for electrical initiation of reentry in normal canine myocardium. J Clin Invest 1989;83:1039–1052.
[73] El-Sherif N. Reentrant mechanisms in ventricular arrhythmias. In: DB Zipe, Jalife J, eds. Cardiac Electrophysiology. From Cell to Bedside. Philadelphia: W.B. Sounders, 1995;567–582.
[74] Fast VG, Pertsov AM. Drift of a vortex in the myocardium. Biophysics 1990;35:489–494.
[75] Abildskov JA, Lux RL. The mechanism of simulated torsade de pointes in a computer model of propagated excitation. J Cardiovasc Electrophysiol 1991;2:224–237.
[76] Panfilov AV, Vasiev BN. Vortex initiation in a heterogeneous excitable medium. Physica D 1991;49:107–113.
[77] Rudenko AN, Panfilov AV. Drift and interaction of vortices in two-dimensional heterogeneous active medium. Stud Biophys 1983;98:183–188.
[78] Pertsov AM, Ermakova EA. Mechanism of the drift of spiral wave in an inhomogeneous medium. Biofizika 1988;33:338–342.
[79] Davidenko JM. Spiral wave activity: a possible common mechanism for polymorphic and monomorphic ventricular tachycardias. J Cardiovasc Electrophysiol 1993;4:730–746.
[80] Schalij MJ, Lammers WJEP, Rensma PL, Allessie MA. Anisotropic conduction and reentry in perfused epicardium of rabbit left ventricle. Am J Physiol 1992;263:H1466–H1478.
[81] Pertsov AM, Jalife J. Three-dimensional vortex-like reentry. In: DB Zipe, Jalife J, eds. Cardiac Electrophysiology. From Cell to Bedside. Philadelphia: W.B. Sounders, 1995;403–409.
[82] Panfilov AV, Pertsov AM. Vortex rings in a three-dimensional medium described by reaction–diffusion equations. Dokl AN SSSR 1984;274:58–60.
[83] Winfree AT. Electrical turbulence in three-dimensional heart muscle. Science 1994;266:1003–1006.
[84] Henriquez CS. Simulating the electrical behavior of cardiac tissue using the bidomain model. Crit Rev Biomed Eng 1993;21:1–77.
[85] Wikswo JP. Tissue anisotropy, the cardiac bidomain. and the virtual electrode effect. In: Cardiac Electrophysiology. From Cell to Bedside. Zipe DP, Jalife J, eds. Philadelphia: Saunders, 1995;348–361.
[86] Noble D. A modification of the Hodgkin-Haxley equations applicable to Purkinje fibre action potential and pace-maker potentials. J Physiol (London) 1962;160:317.